Limnol. Oceanogr., 58(2), 2013, 546–554

doi:10.4319/lo.2013.58.2.0546

Anaerobic oxidation of methane in an iron-rich Danish freshwater lake sediment

Katrin á. Norði,[a,*] Bo Thamdrup,[a] and Carsten J. Schubert [b]

[a] Nordic Center for Earth Evolution, Institute of Biology, University of Southern Denmark, Odense M, Denmark
[b] Department of Surface Waters-Research and Management, Swiss Federal Institute of Aquatic Science and Technology (EAWAG), Kastanienbaum, Switzerland

Abstract

Freshwater systems are identified as one of the main natural methane sources, but little is known about the importance of anaerobic oxidation of methane (AOM) in these systems. We investigated AOM in a lake sediment characterized by a high reactive iron content, normal sulfate concentrations in the bottom water (~ 250 μmol L^{-1}), and a relatively deep sulfate penetration of ~ 14 cm, which facilitated the spatial resolution of the zones of methane production and consumption. Methane concentrations, $\delta^{13}C$ methane profiles, and directly measured and modeled AOM rates all consistently demonstrated methane consumption throughout the anoxic, nitrate-free, Fe(III)- and sulfate-containing zone, oxidizing ~ 90% of the diffusive methane flux. Thus, the concentration gradient of methane was steepest at the base of the Fe(III) and sulfate zone and decreased strongly toward the sediment surface; while $\delta^{13}CH_4$ increased from < −80‰ in the methanogenic zone to −48‰ in the surface sediment. Direct measurements demonstrated AOM activity throughout the Fe(III) and sulfate zone. AOM rates peaked at sulfate concentrations below 3 μmol L^{-1}, which suggests a possible coupling of AOM to the reduction of more crystalline Fe(III) oxides. Alternatively, AOM could be coupled to sulfate reduction, which was in turn supported by a cryptic sulfur cycle coupled to Fe(III) reduction. Our results show that AOM can substantially reduce methane emission from freshwater sediments, and the finding of AOM at sulfate concentrations < 3 μmol L^{-1} suggests that AOM could be of greater importance in freshwater systems, and in ancient low-sulfate oceans, than was previously appreciated.

Methane (CH_4) is a strong greenhouse gas of possible significance in temperature regulation of the early Earth (Pavlov et al. 2000), as well as on modern Earth due to rising CH_4 emissions, as a consequence of anthropogenic release. Methane is produced through the breakdown of organic matter, primarily through biological processes. Natural sources of CH_4 to the atmosphere include wetland soils, freshwater and marine sediments, and digestive fermentation in termites and ruminants (U.S. EPA 2010). Freshwater systems (wetlands, streams, and lakes) are responsible for a significant amount of CH_4 and CO_2 emissions, and lakes alone contribute with 6–16% of the global natural CH_4 emission, while the contribution from oceans is ~ 3% (Bastviken et al. 2004; U.S. EPA 2010).

The emission of methane from sediments represents the net outcome of two counteracting processes: Methanogenesis, which takes place in the anoxic part of the sediment, and oxidation of the generated CH_4 through aerobic or anaerobic microbial processes. Anaerobic oxidation of CH_4 (AOM) is known to be coupled to the reduction of sulfate (SO_4^{2-}), nitrate (NO_3^-), or nitrite (NO_2^-; Knittel and Boetius 2009; Ettwig et al. 2010). Most studies of AOM have been conducted with marine sediment, and although the specific biochemical mechanisms have not yet been unraveled, the AOM coupled to sulfate reduction (SR) is a well-documented process, occurring in the sulfate–methane transition zone (SMTZ) in marine sediments, where it is performed by a consortium of archaea and sulfate-reducing bacteria (Iversen and Jørgensen 1985; Boetius et al. 2000). Here the process is evident from the depth distribution of CH_4 and SO_4^{2-} (Reeburgh 1976; Iversen and Jørgensen 1985) and from stable isotopic composition ($\delta^{13}C$) of CH_4 (Alperin et al. 1988), and it can be directly quantified in incubations with $^{14}CH_4$ and $^{35}SO_4^{2-}$ (Iversen and Jørgensen 1985; Treude et al. 2005). AOM coupled to SR efficiently consumes most of the methane produced in marine sediments, but there is little evidence of a role for this process in freshwater sediments, where SR is limited and methanogenesis is favored by sulfate concentrations that are typically 2–3 orders of magnitude lower than in the ocean. Active SO_4^{2-}-dependent AOM was indicated in the sulfidic sediment of Lago di Cadagno based on carbon isotope analyses and the presence of archaea in the clades that are involved in AOM, but the process was only apparent near the sediment surface where the concentration of SO_4^{2-} was > 2 mmol L^{-1} (Schubert et al. 2011).

Other electron acceptors potentially play a bigger role for AOM in freshwater systems. Thus, AOM coupled to denitrification has been described in enrichment cultures of bacteria that appear to utilize a unique O_2-generating pathway (Ettwig et al. 2010). Such denitrifying methanotrophs appear to be widespread in freshwater sediments based on 16S rDNA surveys (Ettwig et al. 2009), but so far the quantitative role of NO_3^-- or NO_2^--dependent AOM in natural settings has not been explored. Thermodynamically, the oxidation of CH_4 through manganese (Mn) or iron (Fe) reduction would also be feasible, and recent studies have seen some indications of such a coupling (Beal et al. 2009; Crowe et al. 2011; Sivan et al. 2011). Stimulation of AOM after the addition of oxidized Mn or Fe was observed in laboratory incubations of SO_4^{2-}-depleted marine sediment (Beal et al. 2009), and iron reduction was suggested to

* Corresponding author: k.a.nordi@gmail.com

convey AOM in a lake sediment where the consumption of downward-diffusing CH_4 was indicated by an increase in $\delta^{13}C$ of CH_4 with depth (Sivan et al. 2011). A coupling of AOM to Mn and/or Fe reduction was also indicated in the water column of the stratified lake Matano, the world's largest known ferruginous basin (Crowe et al. 2011). These studies mention the possibility that the role of Mn and Fe oxide in AOM is indirect through the stimulation of an oxidative sulfur cycle that may supply SO_4^{2-} for AOM coupled to SR.

Despite the significance of freshwater systems as sources for CH_4, not much is known about the importance of AOM in these systems, the relationship between AOM and SO_4^{2-} concentrations, or whether other electron acceptors are directly or indirectly involved in AOM. With the aim of further exploring the potential for AOM in freshwater environments and analyzing the potential role of Fe oxides in AOM, we studied CH_4 cycling in an Fe-rich lake sediment. The sediment was characterized by a relatively deep SO_4^{2-} penetration, which facilitated the resolution of the zone of CH_4 consumption. We combined geochemical measurements with stable carbon isotope analyses and direct rate determination using radiotracers.

Methods

Study site—The study was conducted in Lake Ørn in Jutland, Denmark. The 0.42 km^2 lake has an average depth of 4 m, with a maximum depth of 10.5 m (Skovgaard 2004). High water flow (retention time 18 d) and wind exposure, together with the shallow depth, normally restricts stratification to the deepest part beneath 5–6 m depth (Skovgaard 2004). The lake receives a high input of iron in the form of ochre from the primary tributary Funder Å, estimated to 45 g Fe m^{-2} yr^{-1} (Skovgaard 2004).

Sampling and sample processing—Sampling was carried out near the center of the lake at 4.5 m water depth (56°09.34′N, 9°31.34′E) in March 2011. Additional cores for determination of CH_4 and O_2 distributions were collected at other times (*see* below). The bottom water temperature in March was 8°C. Six sediment cores (50 cm, 7.4 cm inner diameter) were retrieved using a small, hand-operated gravity corer (Kajak sampler). Three cores were used to determine AOM rates and SR rates, and the three other cores were used for stable carbon isotope analysis. All cores were further sampled for porosity, pore-water extraction, and geochemical analyses. The cores were stored at 6°C until further handling within 2 d, and then subsampled at 2 cm intervals in a glove bag filled with N_2. For subsampling, a 6 cm long extension core liner with two 1.5 cm inner diameter side ports located 1 cm below the top was mounted on top of the core liner. The sediment was gently pushed into this extension and first sampled by horizontal sub-coring with cut-off glass syringes through the side ports for either AOM and SR rate determination or isotopic analysis of CH_4 ($\delta^{13}CH_4$). The syringes for AOM and SR were immediately closed with rubber stoppers, thus minimizing the risk of CH_4 escaping. For $\delta^{13}CH_4$, 2 mL of sediment was transferred into a 20 mL glass vial prefilled with 2.5% NaOH, and was then rapidly sealed. Subsequently, the remainder of each 2 cm interval was split for pore-water extraction in 50 mL centrifuge tubes, porosity measurements, iron extraction, and, for cores for $\delta^{13}C$ analysis, for determination of total organic carbon (TOC) and total nitrogen (TN).

Oxygen profiles were measured in a core sampled in September 2011 with a Clark-type microelectrode equipped with a guard cathode and an internal reference (Revsbech 1989). Three profiles were measured in the core at 100 μm depth resolution. Additionally, CH_4 distributions in the sediment were measured in April 2008, June 2009, and October 2009.

Sediment characteristics and pore-water analysis—Sediment density was determined in each core by weighing 1 cm^3 samples from each interval ($n = 3$), and the water content was determined as the weight loss from fresh sediment dried at 105°C for 24 h. Concentrations of TOC and TN were measured on freeze-dried, homogenized, HCl (4.5% w : w)-treated sediment using a carbon, hydrogen, and nitrogen (CHN) analyzer (Thermo Quest CE Instrument NC 2500). The stable carbon-isotope fractionation of TOC was measured on an Isoprime mass spectrometer connected to a CHN analyzer (Thermo Quest CE Instrument NC 2500) on HCl-treated sediment samples. The most readily acid-soluble Fe minerals were extracted with cold 0.5 mol L^{-1} HCl for 1 h on a rotary shaker, and extracted Fe^{3+} and Fe^{2+} were determined with the Ferrozine method (Thamdrup et al. 1994).

Pore water was obtained by centrifugation of the sediment at 4000 × *g* for 10 min. The supernatant was filtered through 0.45 μm cellulose acetate filters under N_2. From all cores, pore water was analyzed for SO_4^{2-}, NO_3^-, H_2S, and Fe^{2+}. Samples for SO_4^{2-}, NO_3^-, and H_2S were fixed with 20 μL zinc acetate (ZnAc; 2% wt), samples for Fe^{2+} were fixed with 10 μL HCl (6 mol L^{-1}), and all samples were frozen until further analysis. From the cores used to determine stable carbon isotope abundances, pore water was analyzed for dissolved inorganic carbon (DIC) and the carbon isotope composition of DIC (δ^{13}C-DIC) was determined in one of these cores. The DIC concentration was measured by flow injection analysis (Hall and Aller 1992), while δ^{13}C-DIC was measured with a Gasbench II linked to a mass spectrometer (MAT 253, Thermo-Fischer) after acidification with phosphoric acid. Concentrations of SO_4^{2-} and NO_3^- were determined by ion chromatography (Dionex ICS-1500). The reliable quantification limit for SO_4^{2-} was estimated to 3 μmol L^{-1}. Sulfate in standards was detectable to 1 μmol L^{-1}, but the variability was high. Concentrations of H_2S were determined spectrophotometrically by the methylene blue method (Cline 1969; detection limit ~ 0.5 μmol L^{-1}). The Fe^{2+} concentration in the pore water was determined with Ferrozine (Thamdrup et al. 1994). Methane was determined by injection of a 200 μL aliquot of the headspace of NaOH-fixed samples in a gas chromatograph with an FID detector (Perkin Elmer). Values of $\delta^{13}CH_4$ were determined by continuous-flow isotope ratio mass spectrometry with a pre-concentration unit (Precon Finnigan) connected to a

Delta XL IRMS (Finnigan). Results are in δ notation: $\delta^{13}C = ([^{13}C/^{12}C_{sample}]/[^{13}C/^{12}C] - 1) \times 1000‰$ referenced against Vienna Pee-Dee Belemnite.

AOM and SR rate measurements—Process rates were determined by incubation with $^{35}SO_4^{2-}$ (Jørgensen 1978) or $^{14}CH_4$ (Iversen and Jørgensen 1985; Treude et al. 2003). The glass syringes with samples for rate measurements were temperature-equilibrated for 1 h at 6°C before injection with radiotracers. The rubber stopper was then briefly removed and the radiotracer was injected along the central axis of the sediment, while slowly pulling back the syringe needle from the far end of the incubation syringe. For SR, each syringe received 5 μL carrier-free $^{35}SO_4^{2-}$ solution ($\sim$ 40 kBq), the samples were incubated for $\sim$ 1.5 h at 6°C in the dark, and the incubations were stopped by mixing the sediment with 15 mL of 20% ZnAc and freezing until analysis. Radiolabeled reduced sulfur species were quantified by single-step chromium reduction (Fossing and Jørgensen 1989), and SR rates were calculated as described by Jørgensen (1978). Syringes for AOM rates received ^{14}C-labeled CH_4 ($^{14}CH_4$ dissolved in water, injection volume 20 μL, activity 0.5 kBq, supplied from American Radiolabeled Chemicals, cleaned with hopcalite and NaOH) and were incubated at 6°C for 8 h. The AOM incubations were stopped by transfer into glass vials prefilled with 5 mL NaOH (2.5% w : w). The vials were closed immediately with a rubber stopper and shaken vigorously. Activities of $^{14}CH_4$ and $^{14}CO_2$ were determined according to Treude et al. (2005), but using phenylethylamine and methanol (1 : 1) as CO_2 trap. The amount of $^{14}CO_2$ recovered in samples was corrected by the amount of $^{14}CO_2$ recovered in controls that were fixed immediately after injection (Treude et al. 2005). AOM rates were calculated according to Treude et al. (2003).

Inverse modeling of pore-water profiles, flux, and energy yield calculations—Net rates of production or consumption of SO_4^{2-} and CH_4 were calculated from the average depth distributions of these species in the same cores as used for rate measurements, using the curve-fitting software Profile (Berg et al. 1998). Boundary conditions for SO_4^{2-} were as follows: fixed concentration at 1 cm depth and no flux at 41 cm, and for CH_4: fixed concentrations at 1 cm and 41 cm depth. The molecular diffusion coefficients used were 6.36×10^{-6} cm^2 s^{-1} and 9.95×10^{-6} cm^2 s^{-1} for SO_4^{2-} and CH_4, respectively, as calculated for 8°C (Schulz and Zabel 2000).

The diffusive flux of CH_4 out of the sediment and net CH_4 production were calculated from linear concentration gradients according to Fick's first law using measured porosity and the same diffusion coefficients as above. The emission rate was calculated using the concentration in bottom water and at 0–2 cm depth, while the production rate was calculated from the steepest gradient at 14–18 cm depth. Fluxes out of the sediment were calculated similarly for profiles measured in April 2008, June 2009, and October 2009, with diffusion coefficients adjusted to in situ temperatures.

Gibbs free-energy yields at in situ conditions were calculated for potential pathways of AOM:

$$CH_4 + SO_4^{2-} \rightarrow HS^- + HCO_3^- + H_2O \qquad \text{(reaction 1)}$$

$$CH_4 + 8FeOOH + 15H^+ \rightarrow 8Fe^{2+} + HCO_3^- + 13H_2O \qquad \text{(reaction 2)}$$

The calculations were performed based on the thermodynamic constants compiled by Stumm and Morgan (1981) with free energies of formation adjusted to 8°C. For Reaction 2, calculations were done for Fe oxyhydroxide in both amorphous form and in the form of goethite, α-FeOOH (ΔG° of -462 kJ mol^{-1} and -488.6 kJ mol^{-1}, respectively). The in situ energy yield was calculated using in situ pH and concentrations of CH_4, SO_4^{2-}, HS^-, Fe^{2+}, and HCO_3^-, assuming activity coefficients of 1 for these species.

Modeling of isotope fractionation—The isotopic enrichment factor associated with CH_4 consumption was estimated from the depth distribution of $\delta^{13}CH_4$ in the consumption zone by means of a numerical reaction-transport model similar to the approach of Alperin et al. (1988). The model imposed a constant rate, R_{12}, of $^{12}CH_4$ consumption ($[^{12}CH_4] = [CH_4] \times (\delta^{13}CH_4/1000 + 1) \times \delta^{13}CH_{4\ PDB} + 1$), in close approximation of the constant rate of CH_4 consumption derived from the CH_4 distribution (*see* Results), and a constant fractionation factor $\alpha = R_{12}/R_{13} \times [^{13}CH_4]/[^{12}CH_4]$, from which the rate of $^{13}CH_4$ consumption is found as $R_{13} = R_{12}/[^{12}CH_4] \times [^{13}CH_4]/\alpha$. This rate expression was entered to the general one-dimensional reaction-transport equation for $^{13}CH_4$ with transport through molecular diffusion and assuming constant porosity, ϕ:

$$\frac{d[^{13}CH_4]}{dt} = \phi D_s \frac{d^2[^{13}CH_4]}{dx^2} - R_{13}$$

This equation was applied in finite-difference approximation by dividing the zone of CH_4 consumption into a number of discrete, equally sized intervals. For boundary conditions, the concentration of $^{13}CH_4$ was fixed at the measured values at x = 1 cm and x = 19 cm. The equation was solved to steady state ($d[^{13}CH_4]/dt = 0$) by iteration for different values of α, and the corresponding values of $\delta^{13}CH_4$ were calculated and compared with those measured.

Results

Sediment characteristics—The sediment was flocculent and organic-rich, with porosity decreasing from 0.93 mL cm^{-3} near the surface to 0.88 mL cm^{-3} at 40–42 cm depth and contents of TOC and TN decreasing from surface values of 17.7% and 1.7%, respectively, to 10.0% and 0.8% in the deepest section (Table 1). This corresponded to an increase in the molar C : N ratio from 11.9 to 13.8 (Table 1).

Oxygen penetrated to 4 mm depth in September 2011, and NO_3^- was only detected in the upper 0–2 cm of the sediment at concentrations < 5 μmol L^{-1} for all samplings

Table 1. Concentrations of total organic carbon (TOC), total nitrogen (TN), the C : N ratio, and the stable carbon isotopic composition of TOC (δ^{13}C-TOC), measured in the sediment of Lake Ørn. Values in parentheses are SD (n = 3).

Depth (cm)	TOC (%)	TN (%)	C : N ratio (mol : mol)	δ^{13}C-TOC (‰)
1	17.7(1.3)	1.7(0.1)	11.9(0.5)	−30.4(0.1)
3	15.7(1.3)	1.6(0.1)	11.5(0.1)	−30.2(0.1)
5	15.3(0.1)	1.5(0.0)	11.6(0.2)	−30.2(0.4)
7	15.0(1.2)	1.5(0.0)	11.6(0.2)	−30.1(0.4)
9	15.1(1.2)	1.4(0.1)	12.4(1.2)	−30.2(0.1)
11	15.1(0.7)	1.3(0.1)	11.7(0.3)	−30.0(0.2)
13	14.0(0.7)	1.3(0.1)	12.5(0.8)	−29.8(0.2)
15	14.4(1.1)	1.2(0.1)	13.9(0.9)	−29.5(0.2)
17	13.1(1.5)	1.1(0.2)	13.9(0.7)	−29.5(0.1)
19	12.1(1.2)	1.1(0.1)	13.1(0.5)	−29.7(0.1)
21	11.9(1.1)	1.0(0.1)	13.3(0.3)	−29.5(0.2)
23	12.1(1.2)	1.1(0.2)	13.1(0.6)	−29.3(0.6)
25	12.5(0.7)	1.1(0.1)	13.7(0.3)	−29.4(0.3)
27	11.4(0.8)	1.0(0.1)	13.7(0.1)	−29.2(0.1)
29	11.4(0.7)	1.0(0.1)	13.7(0.2)	−29.2(0.2)
31	11.1(0.8)	1.0(0.1)	13.2(0.9)	−29.3(0.3)
33	10.3(0.7)	0.9(0.1)	13.8(0.4)	−29.4(0.2)
35	10.3(0.4)	0.9(0.1)	13.9(0.3)	−29.4(0.3)
37	11.0(0.8)	0.9(0.1)	13.8(0.3)	−29.5(0.1)
39	11.0(1.0)	1.0(0.2)	13.2(1.0)	−29.6(0.1)
41	10.0(0.5)	0.8(0.0)	13.8(0.3)	−29.5(0.2)

(data not shown). The high input of Fe to Lake Ørn was reflected in high concentrations of HCl-extractable iron, increasing from 106 μmol cm^{-3} at 0–2 cm to $\sim$ 661 μmol cm^{-3} at 32–34 cm depth (data not shown). The concentration of HCl-extractable Fe(III) decreased through the upper 12–14 cm of the sediment from 65 μmol cm^{-3} to a low background level of $\leq$ 15 μmol cm^{-3}, which persisted throughout the cores (Fig. 1A). Dissolved Fe^{2+} increased from 42 μmol L^{-1} at 0–2 cm to 649 μmol L^{-1} at 32–34 cm depth (Fig. 1B). Similar to Fe(III), SO_4^{2-} decreased in concentration from 258 μmol L^{-1} in the bottom water to $<$ 4.0 μmol L^{-1} below 14 cm depth (Fig. 1C). Although the concentrations below 14 cm were generally below the reliable quantification limit (3 μmol L^{-1}; *see* Methods), SO_4^{2-} was detected in a few samples to 38 cm depth at concentrations up to 9 μmol L^{-1}. Given the irregularity of SO_4^{2-} distributions below 14 cm, we interpret the occasional detection of SO_4^{2-} here as the result of oxidation during sediment and pore-water handling, although care was taken to avoid contact with O_2 during sampling and filtration. In our experience, even brief exposure of the sediment to air may result in the accumulation in several micromolar of SO_4^{2-} (data not shown). The concentration of H_2S was low with a small peak of 1.2 μmol L^{-1} near the depth of SO_4^{2-} and Fe(III) depletion at 14 cm depth (data not shown).

Methane increased in concentration with depth, with the steepest gradient around 15 cm depth and reaching levels close to saturation at 30 cm (Fig. 1D). This distribution indicated net consumption at depths where Fe(III) and SO_4^{2-} were present and net production below. Application of the curve-fitting program Profile showed that the distribution could be fitted assuming a zone of CH_4 production at a constant rate of 1.31 nmol cm^{-3} d^{-1} from 21 cm to 41 cm, and a zone of CH_4 oxidation at a rate of 1.84 nmol cm^{-3} d^{-1} from 0 cm to 21 cm depth (Fig. 2B). In March 2011, the diffusive flux of CH_4 out of the sediment was calculated to 0.04 mmol m^{-2} d^{-1} corresponding to 11.1% of the integrated CH_4 production (Table 2). A similar CH_4 distribution was measured in April 2008, while the CH_4 front was closer to the surface in June 2009 and had retreated again in October 2009, which suggests some seasonal variation (Fig. 3A). Methane fluxes out of the sediment were calculated to 0.03 mmol m^{-2} d^{-1}, 0.66 mmol m^{-2} d^{-1}, and 0.09 mmol m^{-2} d^{-1} for April 2008, June 2009, and October 2009, respectively, corresponding to 3.8%–50.1% of the flux at the depth of the steepest gradient.

Sulfate reduction and methane oxidation rates—Similar SR rates were measured with ^{35}S tracer in the three different cores, with some variation in the depth distribution (Fig. 2A). The ^{35}S tracer method is much dependent on the SO_4^{2-} concentrations measured in the cores, and therefore the SR rates measured in the deeper part of the sediment (i.e., below 14 cm) have a large uncertainty and

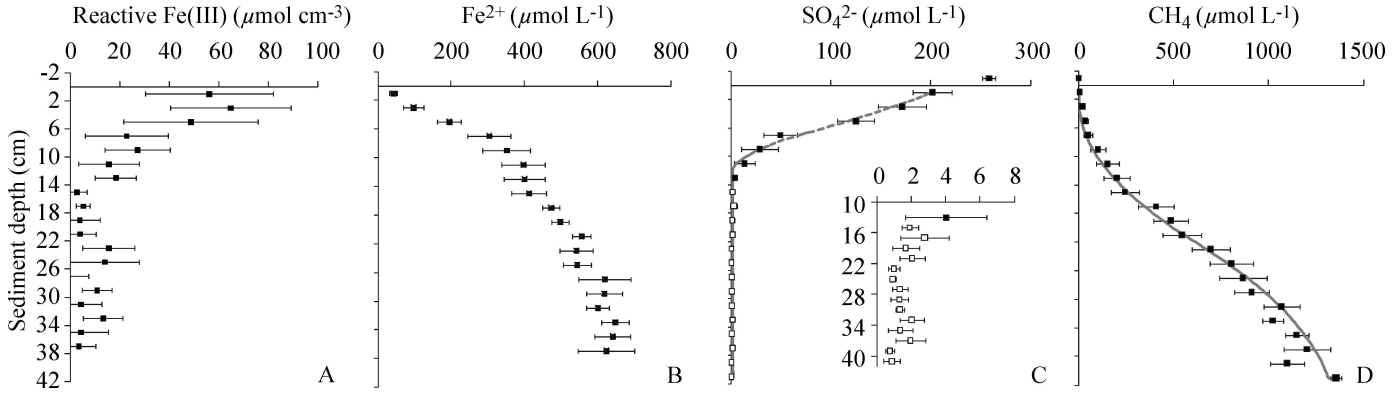

Fig. 1. Geochemical profiles in the sediment of Lake Ørn (mean ± SD; n = 6). (A) Highly reactive, HCl-extractable Fe(III); (B) dissolved Fe^{2+} in pore water; (C) sulfate (open squares show average concentrations below the reliable quantification limit of 3 μmol L^{-1}), and modeled sulfate concentrations (line; n = 6); (D) methane and modeled methane concentrations (line; n = 6).

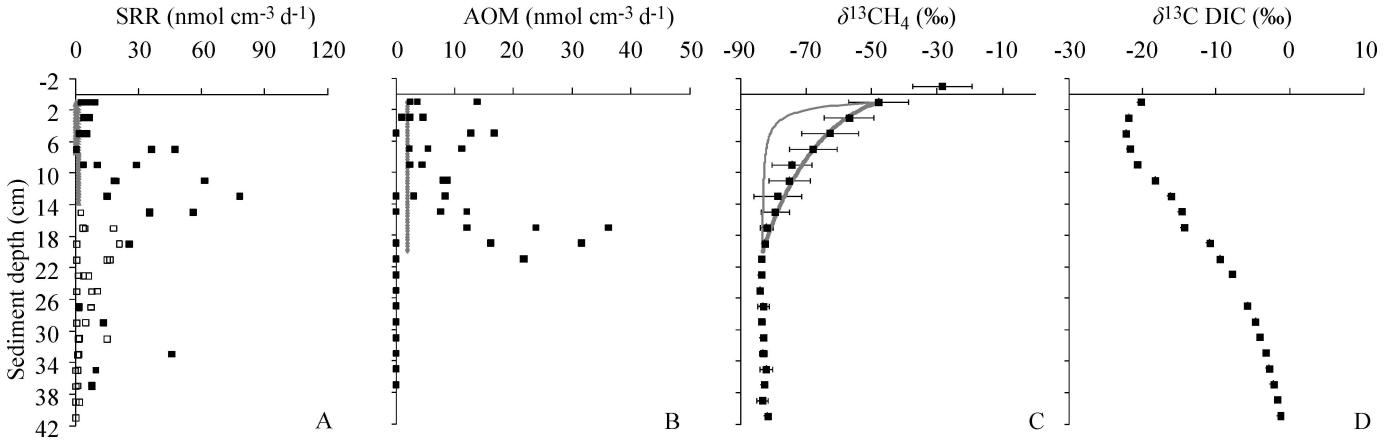

Fig. 2. (A) Measured sulfate reduction rates (SRR; squares; $n = 3$) and SRR derived from the distribution of sulfate in the same cores used for SRR determination (line). Open squares are rates measured at sulfate concentrations below the quantification limit of 3 μmol L^{-1}. (B) Rates of anaerobic oxidation of methane measured directly (squares; $n = 3$) and derived from the distribution of CH_4 (line). (C) Carbon isotope composition of methane ($\delta^{13}CH_4$; mean ± SD; $n = 3$). Curves show model-derived isotopic composition of CH_4 assuming different isotope fractionation factors (α; *see* text for details). From left to right: thin grey curve: $\alpha = 1$ (no fractionation) and thick grey curve: $\alpha = 1.03$. (D) Carbon isotope composition ($\delta^{13}C$) of dissolved inorganic carbon (DIC; $n = 1$).

are easily overestimated, because SO_4^{2-} concentrations below 14 cm fluctuated around the reliable detection limit (*see* Methods). Although SO_4^{2-} concentrations were highest in the upper 6 cm of the sediment (Fig. 1C), SR rates were highest at 6–14 cm depth in all three cores, with a maximum rate of 78 nmol cm^{-3} d^{-1}, indicating a suppression of SR in the upper 6 cm due to the high reactive Fe(III) concentrations (Fig. 1A). The depth-integrated SR rate from 7 cm to 14 cm was 2.2 ± 0.9 mmol m^{-2} d^{-1} ($n = 3$; Table 2). SR rates derived from the SO_4^{2-} profiles showed a similar depth distribution to the ^{35}S-based rates, but were substantially lower (Fig. 2A), with a depth-integrated rate of 0.2 mmol m^{-2} d^{-1}, ~ 12 times lower than the rate obtained with radiotracer (Table 2).

Rates of anaerobic CH_4 oxidation measured with $^{14}CH_4$ showed active AOM in the upper 22 cm of the sediment, corresponding well with the AOM zone derived from the pore-water profiles (Fig. 2B). The highest mean rates of measured AOM, with maximum of 36 nmol cm^{-3} d^{-1} (Fig. 2B), were located at 16–20 cm depth (i.e., in or slightly below the SMTZ). Depth-integrated AOM rates in the upper 21 cm of the sediment were 1.8 ± 0.4 mmol m^{-2} d^{-1}, ~ 5 times higher than the modeled rate (Table 2).

Stable carbon isotopes—The isotope composition, $\delta^{13}C$, of DIC decreased from −20.3‰ at the surface to −22.3‰ at 4–6 cm depth, but then increased steadily to −1.3‰ at 40–42 cm depth (Fig. 2D), while the $\delta^{13}C$ of TOC increased slightly with depth from −30.4‰ to −29.5‰ (Table 1). The $\delta^{13}C$ CH_4 was relatively uniform and strongly depleted in ^{13}C below 16 cm depth, with a slight downward increase from −84.1‰ at 24–26 cm to −81.7‰ at 40–42 cm (Fig. 2C). Above 16 cm depth, the values became increasingly heavy (i.e., less negative) reaching −48.0‰ at 0–2 cm (Fig. 2C). Reaction-transport modeling of $\delta^{13}CH_4$ in the zone of CH_4 oxidation yielded the best fit to the measured $\delta^{13}CH_4$ values with an enrichment factor, α, of 1.030, while the distribution obtained for $\alpha = 1.000$ (no fractionation) deviated strongly from the measurements (Fig. 2C).

Discussion

Redox zonation—The vertical distribution of electron acceptors in the sediment of Lake Ørn was consistent with the order of decreasing free-energy yield, and the zonation was relatively deep. Oxygen respiration was restricted to the upper 4 mm, and NO_3^- was likely depleted just below the O_2 depletion zone and certainly below 2 cm (the depth resolved in our sampling). This leaves Fe(III) and SO_4^{2-} as the main electron acceptors below 2 cm depth. The relatively high concentration of poorly crystalline iron in the upper part of the sediment (Fig. 1A), and the

Table 2. Methane emission, production, anaerobic oxidation rates (AOM), and sulfate reduction rates (SRR) obtained from flux calculations from Fick's first law, curve-fitting model, and direct measurements.

	Calculated flux (mmol m^{-2} d^{-1})	Modeled rates (mmol m^{-2} d^{-1})	Measured rates (mmol m^{-2} d^{-1})
CH_4 emission	0.04	—	—
CH_4 production	0.36	0.26	—
AOM	0.32*	0.36	1.82±0.41
SRR†	—	0.18	2.23±0.88

* Production minus emission.
† Depth-integrated rates at 7–14 cm.

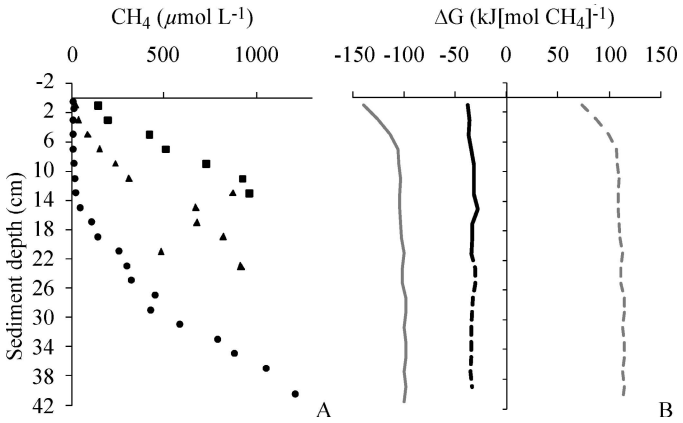

Fig. 3. (A) Methane concentration profiles in Lake Ørn sediment in April 2008 (circles), June 2009 (squares), and October 2009 (triangles). (B) Gibbs free-energy yield (ΔG) calculated for the anaerobic oxidation of methane (AOM) coupled to sulfate reduction (black line), and AOM coupled to Fe(III) reduction using amorphous FeOOH (grey line) or α-FeOOH (goethite; grey stippled line) for pore-water concentrations found in March 2011. The black stippled line indicates values at depths where sulfate concentrations were at or below the reliable quantification limit (3 μmol L^{-1}).

suppression of SR to below 6 cm depth or deeper seen in both ^{35}S-based and modeled rates (Fig. 2A), indicates that Fe reduction was the dominating terminal electron-accepting process in a zone of $\geq$ 4 cm thickness. This is consistent with results from other freshwater sediments that showed the dominance of Fe reduction at similar concentrations of poorly crystalline Fe(III; Roden and Wetzel 1996; Thomsen et al. 2004).

There was no clear distinction between the depths where HCl-extractable Fe(III) and SO_4^{2-} reached background levels, but the agreement between this depth and the onset of net CH_4 production as indicated by the CH_4 distribution (Fig. 1D), confirmed that these electron acceptors were depleted to such an extent that methanogenesis prevailed. The Fe(III) measured here represents only the poorly crystalline fraction of Fe oxides, which is preferred by dissimilatory iron-reducers, while the HCl-extraction does not dissolve more crystalline Fe(III) oxides (Lovley and Phillips 1987*a*,*b*). The continued increase in soluble Fe^{2+} (Fig. 1B) and HCl-extractable Fe(II) below 14 cm depth indicates that Fe(III) pools not dissolved by the HCl extraction persisted to greater depth as observed in other sediments (Thamdrup et al. 1994). Also the very slight accumulation of H_2S indicates the presence of reactive Fe scavenging H_2S to the depth of SO_4^{2-} depletion. The deep penetration of SO_4^{2-} in Lake Ørn is unusual for shallow, eutrophic lakes with micromolar levels of sulfate in the water (Holmer and Storkholm 2001), but the redox zonation was comparable to that reported for a 100 m deep site in Lake Michigan, where reactive Fe(III) also reached similar depth as SO_4^{2-} (Thomsen et al. 2004).

Evidence for AOM—The distribution of CH_4 in the sediment of Lake Ørn provided initial evidence for AOM several centimeters below the sediment surface (Fig. 1D). Although the concentrations of CH_4 were high in the deeper part of the sediment, the concave shape of the CH_4 profile indicated consumption through the anoxic, Fe(III)- and SO_4^{2-}-containing zone with little CH_4 escaping to the bottom water. Indeed, a SMTZ analogous to the one known from marine sediments was clearly identified in all cores from March 2011.

Further evidence for AOM was the systematic shift in stable carbon isotopic composition of CH_4 (Fig. 2C; Alperin et al. 1988; Whiticar 1999). Methanogenesis and AOM have opposite effects on $\delta^{13}CH_4$ because $^{12}CH_4$ is preferentially formed and consumed, and the fractionation against the heavier isotope has been demonstrated for both aerobic (Barker and Fritz 1981) and anaerobic oxidation (Holler et al. 2009). The isotopic composition of CH_4 in the zone of methanogenesis in Lake Ørn was $\sim$ 54‰ and 72‰ lighter than $\delta^{13}C$ of organic C and DIC, respectively (Table 1; Fig. 2D). The large isotopic shift between DIC and CH_4 is consistent with H_2-based CO_2 reduction as the dominant methanogenic pathway as often observed in lake sediments (Conrad 1999), while the fractionation during acetoclastic methanogenesis is $\sim$ 24–27‰ (Whiticar 1999). The large positive shift of $\delta^{13}CH_4$ of 36‰ from the upper part of the methanogenic zone to near the sediment surface thus provides strong evidence for CH_4 consumption associated with isotopic fractionation during upward transport through the anoxic Fe(III)- and SO_4^{2-}-containing zone. This was confirmed by application of a reaction-transport model, which yielded the best fit to our measurements with an enrichment factor α = 1.030 (Fig. 2C). This value is within the range found for AOM in enrichment cultures (α = 1.012–1.039; Holler et al. 2009) and similar to that inferred for AOM in an anoxic, SO_4^{2-}-rich alpine lake (α = 1.031; Schubert et al. 2011).

Finally, direct measurement of AOM provided evidence of anaerobic oxidation of CH_4 in the upper 22 cm of the sediment, with the highest rates at 16–20 cm depth (Fig. 2B). The zone of measured AOM was consistent with the zone of AOM derived from the distribution of CH_4, considering that the program used for interpreting CH_4 distributions is not designed to resolve fine structure in the depth distribution of rates such as the deep peak in AOM seen in the direct measurements (Berg et al. 1998). The depth-integrated measured rate was $\sim$ 5 times higher than the modeled rate (Table 1). Such discrepancies have been found before, although the two methods matched reasonably in other cases (Iversen and Jørgensen 1985; Alperin et al. 1988). Several factors may contribute to this difference. The reactive-transport model assumes steady state, while rates were likely increasing due to the increasing temperature and higher carbon input when sediment was sampled in spring. This could lead to an underestimation of the AOM by the model. Furthermore, the model only yields net rates, and any overlap between production and consumption of CH_4 would also lead to underestimation of AOM in the model. Bio-irrigation may potentially also affect the modeling, but fauna was sparse and not seen below 5 cm depth. The AOM rates measured in Lake Ørn were in the same range as were found in coastal and margin SMTZ (Knittel and Boetius 2009).

In summary, the distribution of CH_4 in the sediment (Fig. 1D), the $\delta^{13}CH_4$ profile (Fig. 2C), and direct measured and modeled AOM rates (Fig. 2B) all consistently demonstrated that CH_4 oxidation in the anoxic part of the sediment above ~ 20 cm depth. To our knowledge, this is the first study showing AOM in freshwater sediment supported by profiles, stable carbon isotope analyses, and direct AOM rate measurements, and also the first example of freshwater sediment where most of the diffusive CH_4 flux is consumed by anaerobic oxidation within the sediment. We did not investigate AOM over a seasonal cycle, but the distribution of CH_4 at other times of sampling (Fig. 3A) suggests that our findings are at least representative of spring, while the CH_4 front seems to reach the surface during summer and recede into the sediment during autumn.

Oxidants for anaerobic oxidation of methane—It is difficult to distinguish which of the two electron acceptors (Fe(III) and SO_4^{2-}) could be responsible for the observed AOM. In the zone where AOM was most active (16–22 cm), both poorly crystalline Fe(III) and SO_4^{2-} concentrations had reached background values of ~ 15 μmol cm^{-3} and $\leq$ 3 μmol L^{-1}, respectively (Fig. 1A and C). A closer inspection of the SO_4^{2-} profile suggests a tail of low SO_4^{2-} extending to 22 cm (Fig. 1C), but as discussed in Methods, we do not fully trust the quantification at these levels. To our knowledge, these are the lowest documented SO_4^{2-} concentrations at which AOM has been measured directly. AOM was previously detected in marine sediment with SO_4^{2-} depleted below a detection limit of 30 μmol L^{-1} (Beal et al. 2011).

As argued above, the continued accumulation of Fe(II) with depth indicates the reduction of more crystalline Fe(III) phases, which potentially serve as oxidant in AOM in Lake Ørn. However, AOM coupled to SR is thermodynamically favorable even at the low SO_4^{2-} concentrations observed in Lake Ørn, where the energy yield for AOM coupled to SR ranged from −38 kJ mol^{-1} to −31 kJ mol^{-1} (Fig. 3B). This range of yields is similar to yields of −22 to −35 kJ mol^{-1} reported for locations where AOM coupled to SO_4^{2-} is known to occur (Caldwell et al. 2008). The energy yield from AOM coupled to iron reduction depends strongly on the form of iron oxide (Fig. 3B). With amorphous Fe(III) oxide, targeted by our HCl extraction, and at the concentrations of other involved species as found in Lake Ørn, the yield is much larger than with SO_4^{2-}; whereas, the process would not be favorable with crystalline goethite. The depletion of both HCl-extractable Fe(III) and SO_4^{2-} in the deepest part of the AOM zone indicates that amorphous Fe oxide was depleted and that the residual Fe(III) oxide was not a more favorable electron acceptor than SO_4^{2-}.

Although SO_4^{2-}-driven AOM would be thermodynamically feasible, and a tail of low SO_4^{2-} concentrations possibly extended to the bottom of the AOM zone at 22 cm (Fig. 1C), the rates of SR derived from SO_4^{2-} distributions assuming diffusion and reaction (Fig. 2A) clearly showed that AOM in the deepest part of the zone could not be supported by a diffusive flux of SO_4^{2-} from above. However, SO_4^{2-} may have been supplied from a cryptic sulfur cycle at the same depths where it was consumed. Evidence for reoxidation of sulfide in the sediment came from the large, 12-fold difference between measured and modeled SR (Fig. 2A). Although other factors may contribute to this difference, as discussed for the offset in modeled and measured AOM rates above, the difference was much larger than for AOM. Indeed, it seems typical for freshwater sediments that directly measured rates of SR substantially exceed those supported by diffusion, and this has been attributed to rapid reoxidation of sulfide (Urban et al. 1994). The mechanisms of reoxidation could involve cycles of abiotic oxidation of sulfide to elemental sulfur with Fe(III) oxide coupled to disproportionation of sulfur to sulfide and SO_4^{2-} (Thamdrup et al. 1993). Such cycles were also proposed to support a cryptic sulfur cycle in the CH_4 zone of marine sediment (Holmkvist et al. 2011). Although SR rates below 14 cm were not trusted due to SO_4^{2-} concentrations at or below the quantification limit, the measurements show a potential for SR toward the bottom of the AOM zone at rates similar to the measured AOM rates (Fig. 2A). The ratio of SR to AOM at 14–22 cm depth was 0.4–1.5, which would be consistent with the general 1 : 1 coupling of SR to AOM, all uncertainties considered.

Based on the analysis above, we conclude that SO_4^{2-} is just as likely to be the oxidant for AOM in Lake Ørn as is Fe(III) oxide: the process is thermodynamically feasible, SR is active, and there is no indication of preferential reduction of Fe(III) in the deeper part of the AOM zone. If Fe(III) oxide is available for AOM it is also available for abiotic reaction with sulfide, and SO_4^{2-} can be regenerated by disproportionation of the oxidation products. AOM coupled to SO_4^{2-} reduction is a well-documented process, while AOM coupled to Fe reduction has been suggested but not conclusively proven. Thus, the more parsimonious explanation for our observations is that AOM was coupled to SR that was supported by a cryptic sulfur cycle coupled to Fe(III) reduction. Investigations of the microbiology of the process may provide further insights into the role of SO_4^{2-} and Fe(III) as electron acceptors.

Our results show that AOM can play a substantial role in regulating the flux of CH_4 from sediments in waters with SO_4^{2-} concentrations typical for freshwaters. Although the sediment of Lake Ørn is extraordinarily rich in iron, the process proceeded at depths where both poorly crystalline iron and SO_4^{2-} were close to depletion, which suggests that it may also be of importance in less iron-rich sediments. Our results further support indications of AOM in hypolimnia of monomictic lakes (Eller et al. 2005; Schubert et al. 2010), although they contrast with those from sediment of Lake Cadagno (where AOM was only indicated at SO_4^{2-} concentrations above 1.5 mmol L^{-1}; Schubert et al. 2011). In this monomictic lake, high sulfide concentrations might affect the thermodynamics of the process adversely. Further investigations are clearly required to quantify the role of AOM in the CH_4 cycle of different types of freshwater environments.

Anoxic, iron-rich, and sulfate-poor conditions likely dominated the oceans through much of Earth's early history, and iron oxides were available as electron acceptors in underlying sediments (Konhauser at al. 2005). Thus, our

finding of active AOM in the presence of iron oxides at low sulfate concentrations results further supports the hypothesis that AOM could have played a role in the regulation of methane emission from the ancient ocean (Beal et al. 2009; Crowe et al. 2011). Also in this context, it will be important to elucidate whether AOM is coupled directly to iron reduction or to a cryptic sulfur cycle.

Acknowledgments

We thank Gijs Nobbe and Heidi Grøn Jensen for their support in the laboratories in Kastanienbaum and Odense, respectively. Stefano Bernasconi at Eidgenössische Technische Hochschule is thanked for measuring carbon stable isotopes on inorganic carbon. This study was supported by the Danish National Research Foundation, the Danish Council for Independent Research and Swiss Federal Institute of Aquatic Science and Technology. Tina Treude and two anonymous reviewers are thanked for their comments to the manuscript.

References

Alperin, M. J., W. S. Reeburgh, and M. J. Whiticar. 1988. Carbon and hydrogen isotope fractionation resulting from anaerobic methane oxidation. Glob. Biogeochem. Cycles **2:** 279–288, doi:10.1029/GB002i003p00279

Barker, J. F., and P. Fritz. 1981. Carbon isotope fractionation during microbial methane oxidation. Nature **293:** 289–291, doi:10.1038/293289a0

Bastviken, D., J. Cole, M. Pace, and L. Tranvik. 2004. Methane emissions from lakes: Dependence of lake characteristics, two regional assessments, and a global estimate. Glob. Biogeochem. Cycles **18:** GB40009, doi:10.1029/2004GB002238

Beal, E. J., M. W. Claire, and C. H. House. 2011. High rates of anaerobic methanotrophy at low sulfate concentrations with implications for past and present methane levels. Geology **9:** 131–139.

———, C. H. House, and V. J. Orphan. 2009. Manganese- and iron-dependent marine methane oxidation. Science **325:** 184–187, doi:10.1126/science.1169984

Berg, P., N. Risgaard-Petersen, and S. Rysgaard. 1998. Interpretation of measured concentration profiles in sediment pore water. Limnol. Oceanogr. **43:** 150–151, doi:10.4319/lo.1998.43.7.1500

Boetius, A., and others. 2000. A marine microbial consortium apparently mediating anaerobic oxidation of methane. Nature **407:** 623–626, doi:10.1038/35036572

Caldwell, S. L., J. R. Laidler, E. A. Brewer, J. O. Eberly, S. C. Sandborgh, and F. S. Colwell. 2008. Anaerobic oxidation of methane: Mechanisms, bioenergetics, and the ecology of associated microorganisms. Environ. Sci. Technol. **42:** 6791–6799, doi:10.1021/es800120b

Cline, J. D. 1969. Spectrophotometric determination of hydrogen sulfide in natural waters. Limnol. Oceanogr. **14:** 454–458, doi:10.4319/lo.1969.14.3.0454

Conrad, R. 1999. Contribution of hydrogen to methane production and control of hydrogen concentrations in methanogenic soils and sediment. FEMS Microbiol. Ecol. **28:** 193–202, doi:10.1111/j.1574-6941.1999.tb00575.x

Crowe, S. A., and others. 2011. The methane cycle in ferruginous Lake Matano. Geobiology **9:** 61–78, doi:10.1111/j.1472-4669.2010.00257.x

Eller, G., L. Känel, and M. Krüger. 2005. Cooccurrence of aerobic and anaerobic methane oxidation in the water column of Lake Plussee. Appl. Environ. Microbiol. **71:** 8925–8928, doi:10.1128/AEM.71.12.8925-8928.2005

Ettwig, K. F., and others. 2010. Nitrate-driven anaerobic methane oxidation by oxygenic bacteria. Nature **464:** 543–550, doi:10.1038/nature08883

———, T. van Alen, K. T. van de Pas-Schoonen, M. S. M. Jetten, and M. Strous. 2009. Enrichment and molecular detection of denitrifying methanotrophic bacteria of the NC10 phylum. Appl. Environ. Microbiol. **75:** 3656–3662, doi:10.1128/AEM.00067-09

Fossing, H., and B. B. Jørgensen. 1989. Measurement of bacterial sulfate reduction in sediments: Evaluation of a single-step chromium reduction method. Biogeochemistry **8:** 205–222, doi:10.1007/BF00002889

Hall, P. O. J., and R. C. Aller. 1992. Rapid, small-volume, flow injection analysis for $\sum CO_2$ and $\sum NH_4$ in marine and freshwaters. Limnol. Oceanogr. **37:** 1113–1119, doi:10.4319/lo.1992.37.5.1113

Holler, T., G. Wegener, K. Knittel, A. Boetius, B. Grunner, M. M. M. Kuypers, and F. Widdel. 2009. Substantial $^{13}C/^{12}C$ and D/H fractionation during anaerobic oxidation of methane by marine consortia enriched in vitro. Environ. Microbiol. Rep. **1:** 370–376, doi:10.1111/j.1758-2229.2009.00074.x

Holmer, M., and P. Storkholm. 2001. Sulphate reduction and sulphur cycling in lake sediments: A review. Freshw. Biol. **46:** 431–451, doi:10.1046/j.1365-2427.2001.00687.x

Holmkvist, L., T. G. Ferdelman, and B. B. Jørgensen. 2011. A cryptic sulfur cycle driven by iron in the methane zone of marine sediment (Aarhus Bay, Denmark). Geochim. Cosmochim. Acta **75:** 3581–3599, doi:10.1016/j.gca.2011.03.033

Iversen, N., and B. B. Jørgensen. 1985. Anaerobic methane oxidation rates at the sulfate–methane transition in marine sediments from Kattegat and Skagerrak (Denmark). Limnol. Oceanogr. **30:** 944–955, doi:10.4319/lo.1985.30.5.0944

Jørgensen, B. B. 1978. A comparison of methods for the quantification of bacterial sulfate reduction in coastal marine sediments. I. Measurement with radiotracer techniques. Geomicrobiol. J. **1:** 11–27, doi:10.1080/01490457809377721

Knittel, K., and A. Boetius. 2009. Anaerobic oxidation of methane: Progress with an unknown process. Ann. Rev. Microbiol. **63:** 311–334, doi:10.1146/annurev.micro.61.080706.093130

Konhauser, K. O., D. K. Newman, and A. Kappler. 2005. The potential significance of microbial Fe (III) reduction during deposition of Precambrian banded iron formations. Geobiology **3:** 167–177, doi:10.1111/j.1472-4669.2005.00055.x

Lovley, D. R., and E. J. P. Phillips. 1987*a*. Competitive mechanisms for inhibition of sulfate reduction and methane production in the zone of ferric iron reduction in sediments. Appl. Environ. Microbiol. **53:** 2636–2641.

———, and ———. 1987*b*. Rapid assay for microbially reducible ferric iron in aquatic sediments. Appl. Environ. Microbiol. **53:** 1536–1540.

Pavlov, A. A., J. F. Kasting, L. L. Brown, K. A. Rages, and R. Freedman. 2000. Greenhouse warming by CH_4 in the atmosphere of early Earth. J. Geophys. Res. Planets **105:** 11981–11990, doi:10.1029/1999JE001134

Reeburgh, W. S. 1976. Methane consumption in Cariaco Trench waters and sediment. Earth Planet. Sci. Lett. **28:** 337–344, doi:10.1016/0012-821X(76)90195-3

Revsbech, N. P. 1989. An oxygen microsensor with a guard cathode. Limnol. Oceanogr. **34:** 474–478, doi:10.4319/lo.1989.34.2.0474

Roden, E. E., and R. G. Wetzel. 1996. Organic carbon oxidation and suppression of methane production by microbial Fe(III) oxide reduction in vegetated and unvegetated freshwater sediments. Limnol. Oceanogr. **41:** 1733–1748, doi:10.4319/lo.1996.41.8.1733

Schubert, C. J., and others. 2010. Oxidation and emission of methane in a monomictic lake (Rotsee, Switzerland). Aquat. Sci. **72:** 455–466, doi:10.1007/s00027-010-0148-5

———, F. Vazquez, T. Losenkann-Behrens, K. Knittel, M. Tonolla, and A. Boetius. 2011. Evidence for anaerobic oxidation of methane in sediments of a freshwater system (Lago di Cadagno). FEMS Microbiol. Ecol. **76:** 26–38, doi:10.1111/j.1574-6941.2010.01036.x

Schulz, H., and M. Zabel. 2000. Marine geochemistry. Springer.

Sivan, O., M. Adler, A. Pearson, F. Gelman, I. Bar-Or, S. C. John, and W. Eckert. 2011. Geochemical evidence for iron-mediated anaerobic oxidation of methane. Limnol. Oceanogr. **56:** 1536–1544, doi:10.4319/lo.2011.56.4.1536

Skovgaard, H. 2004. Ørn Sø 2003. Environmental monitoring report, County of Aarhus.

Stumm, W., and J. Morgan. 1981. Aquatic chemistry, 2nd ed. Wiley.

Thamdrup, B., K. Finster, J. W. Hansen, and F. Bak. 1993. Bacterial disproportionation of elemental sulfur coupled to chemical reduction of iron or manganese. Appl. Environ. Microbiol. **59:** 101–108.

———, H. Fossing, and B. B. Jørgensen. 1994. Manganese, iron, and sulfur cycling in a coastal marine sediment, Aarhus Bay, Denmark, Geochim. Cosmochim. Acta **58:** 5115–5129, doi:10.1016/0016-7037(94)90298-4

Thomsen, U., B. Thamdrup, D. A. Stahl, and D. E. Canfield. 2004. Pathways of organic carbon oxidation in a deep lacustrine sediment, Lake Michigan. Limnol. Oceanogr. **49:** 2046–2057, doi:10.4319/lo.2004.49.6.2046

Treude, T., A. Boetius, K. Knittel, K. Wallmann, and B. B. Jørgensen. 2003. Anaerobic oxidation of methane above gas hydrates at Hydrate Ridge, NE Pacific Ocean. Mar. Ecol. Prog. Ser. **264:** 1–14, doi:10.3354/meps264001

———, M. Kruger, A. Boetius, and B. B. Jørgensen. 2005. Environmental control on anaerobic oxidation of methane in the gassy sediment of Eckernforde Bay (Germen Baltic). Limnol. Oceanogr. **50:** 1771–1786, doi:10.4319/lo.2005.50.6.1771

U.S. Environmental Protection Agency [U.S. EPA]. 2010. Methane and nitrous oxide emissions from natural sources. Report no. EPA-43-R-10-001. Washington, D.C.: EPA Office of Atmospheric Programs.

Urban, N. R., P. L. Brezonik, L. A. Baker, and L. A. Sherman. 1994. Sulfate reduction and diffusion in sediment of Little Rock Lake, Wisconsin. Limnol. Oceanogr. **39:** 797–815, doi:10.4319/lo.1994.39.4.0797

Whiticar, M. J. 1999. Carbon and hydrogen isotope systematic of bacterial formation and oxidation of methane. Chem. Geol. **161:** 291–314, doi:10.1016/S0009-2541(99)00092-3

Associate editor: Mary I. Scranton

Received: 21 May 2012
Accepted: 14 November 2012
Amended: 28 November 2012